Available online at www.sciencedirect.com

ScienceDirect

Ceramics International 39 (2013) 9483–9490

CERAMICS INTERNATIONAL

www.elsevier.com/locate/ceramint

Laser glazing of plasma-sprayed nanostructured yttria stabilized zirconia thermal barrier coatings

Reza Ghasemi*, Reza Shoja-Razavi, Reza Mozafarinia, Hossein Jamali

Department of Materials Engineering, Malek-Ashtar University of Technology, Shahinshahr, Isfahan, Iran

Received 26 April 2013; received in revised form 5 May 2013; accepted 6 May 2013
Available online 24 May 2013

Abstract

Nanostructured thermal barrier coatings (TBCs) consisting of yttria stabilized zirconia (YSZ) ceramic top coat and NiCrAlY metallic bond coat were prepared by atmospheric plasma spraying (APS). The Nd:YAG pulsed laser was used for laser treatment of top coat surface. The microstructure and thermal insulation capability of plasma-sprayed and laser-glazed thermal barrier coatings were investigated. The microstructure and phase composition of the coating were characterized by field emission scanning electron microscopy (FESEM) and X-ray diffractometry (XRD). The nanostructured plasma-sprayed coating contained non-melted or partially melted nanosized particles and columnar grains, whereas the microstructure of laser-glazed coating consisted of columnar grains in the fracture surface and equiaxed grains on the surface. Laser glazing, which helps to eliminate the surface porosities and other structural defects of coatings deposited by the plasma spraying method, should contribute to the improvement of their surface roughness. XRD results revealed that both as-sprayed and laser-glazed coatings consisted of non-transformable tetragonal (T′) phase. The results of the thermal insulation capability test indicated that the thermal insulation capability of the laser-glazed coating, as compared to the as-sprayed coating, was slightly lower due to the microstructural change in the glazed layer of top coat.
© 2013 Elsevier Ltd and Techna Group S.r.l. All rights reserved.

Keywords: Thermal barrier coating; Microstructure; Laser glazing; Atmospheric plasma spraying.

1. Introduction

The hot-section components of advanced aircraft and industrial gas-turbine engines are often coated with a thermal barrier coating to protect them from high temperature degradation and to extend their service life [1–3]. Typically, the TBC system consists of three layers: a ceramic top coat, a metallic bond coat, and a nickel-based superalloy substrate [4,5]. The bond coat typically consists of MCrAlY, where M is a metal such as Ni and/or Co. Bond coat improves adhesion between the ceramic and the substrate, being typically oxidized in service [6,7]. Yttria stabilized zirconia was commonly used as top coat because of high temperature stability in oxidizing and combustion atmospheres, low thermal conductivity, and high thermal expansion coefficient, which closely matches that of the substrate [8–10]. A thermally grown oxide (TGO) is formed at the interface between the bond coat and ceramic top coat due to high temperature oxidation of the bond coat; and the possibility of failure at the interface increases due to various stresses and TGO layers [11,12].

The two main commercial processes now widely used for the deposition of thermal barrier coatings are plasma spraying and electron-beam physical vapor deposition (EB-PVD). APS TBCs have a relatively low application cost, and are generally less durable than EB-PVD TBCs [13,14].

Previous results have demonstrated that the oxidation of bond coat and metal/ceramic thermal linear expansion mismatch during thermal cycling were the main factors that limited the life of thermal barriers coatings. When the thickness of the TGO exceeds a ceramic limit, it induces the critical stress needed for coating failure. Other factors that contribute to the degradation of TBCs are high and low-cycle fatigue, high-temperature erosion, and hot-corrosion [15–17]. In previous studies, a variety of methods have been employed

*Corresponding author. Tel.: +98 3125225041; fax: +98 3125228530.
E-mail addresses: r_ghasemi@mut-es.ac.ir, reza.ghasemi65@gmail.com (R. Ghasemi).

0272-8842/$ - see front matter © 2013 Elsevier Ltd and Techna Group S.r.l. All rights reserved.
http://dx.doi.org/10.1016/j.ceramint.2013.05.066

to modify the properties of the TBCs, including functionality graded material (FGM), surface-sealing treatment such as laser glazing, aluminum phosphate sealing, sol–gel process, and the use of nanostructured material [18,19]. Laser glazing as an advanced processing technique has been used to modify TBCs surface. Laser glazing provides a remelting and succeeding solidification of the surface, resulting in a dense top layer with a new microstructure. It also leads to reducing the surface roughness considerably. Free from porosity, it forms a network of continuous cracks perpendicular to the surface [20–22].

Ahmadi-Pidani [23] reported that the segmented cracks produced by laser glazing were found to improve the strain accommodation, finally leading to fourfold thermal shock lifetime extension of TBCs, in comparison with plasma-sprayed TBCs. Ahmaniemi et al. [24] stated that laser glazing TBCs significantly improved microhardness, abrasion, and erosion resistance, whilst lowering strength and stiffness. Tsia [17] indicated that laser-glazed TBCs exhibited better hot-corrosion resistance than plasma-sprayed TBCs in a V_2O_5 salt containing a corrosive environment due to the reduction of penetration of the molten salts through the dense glazed layer. Studies conducted by Batista [25] reported that the laser glazing could decrease the surface roughness and eliminate the porosity to densify the coatings, while the decrease in voids and microcracks led to an increase in apparent thermal conductivity and a decrease in thermal insulation [26]. Therefore, detailed, systematic studies of the behavior of laser-glazed TBCs seem necessary.

In recent years, much research has been conducted on laser glazing YSZ thermal barrier coatings; however, the as-sprayed YSZ thermal barrier coatings used for laser glazing were mainly prepared using conventional YSZ starting powder. Therefore, the interest is in laser glazing the YSZ thermal barrier coatings by using the nanostructured YSZ agglomerated powders to effectively improve the performance of the TBCs.

2. Materials and methods

2.1. Material

An Ni-based superalloy (Inconel 738LC) was used as the substrate material. The spraying material for the bond coat was microstructured NiCrAlY powder (AMDRY 962, Sulzer Metco Inc., USA, 56–106 μm) with nominal composition of Ni–22Cr–10Al–1.0Y (wt%), as shown in Fig. 1(a) and the top coat was nanostructured yttria stabilized zirconia (ZrO_2–7 wt% Y_2O_3, Nanox S4007, Inframet Corp., Farmington, CT, 15–150 μm) as shown in Fig. 1(b). It is clearly observed from Fig. 1(b) that the powder particles are spherical. When the surface of this particle is analyzed at higher magnification, it is possible to observe the nanostructure of the feedstock (Fig. 1 (c)), each microscopic YSZ particle is formed via the agglomeration of individual YSZ particles smaller than 100 nm. The X-ray diffraction patterns of the nanostructured YSZ powder are shown in Fig. 2. The grain size was determined on the basis of the Scherrer equation using the two high intensity peaks located at low angles:

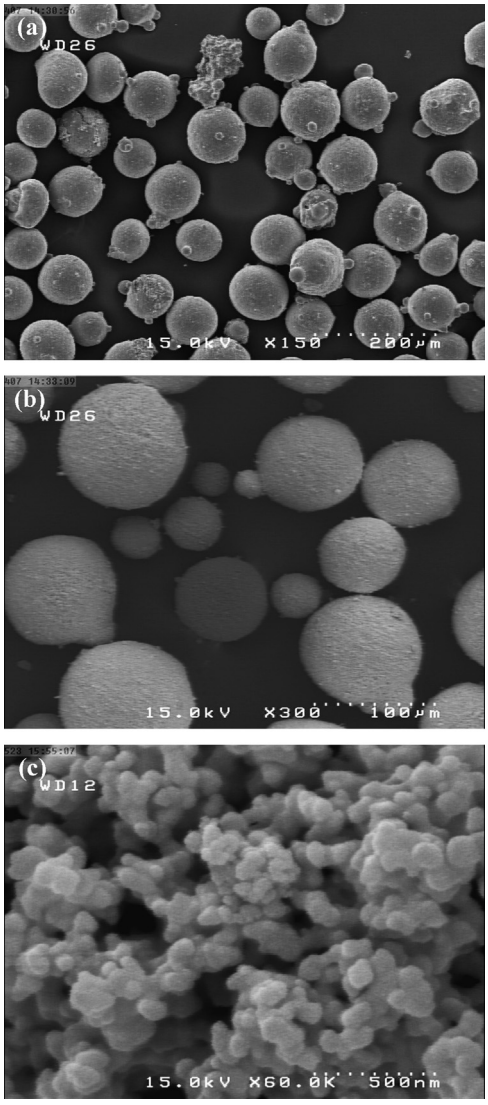

Fig. 1. FESEM micrographs of starting powder: (a) NiCrAlY powder, (b) outer surface of agglomerated nanostructured YSZ powder and (c) internal morphology of a nanostructured YSZ powder at a higher magnification; individual nanosized YSZ particles smaller than 100 nm.

$$B(2\theta) = 0.9\lambda/D\cos\ \theta \quad (1)$$

where D is the average diameter dimensions of crystallites, B is the broadening of the diffraction line measured at half maximum intensity, λ is the wavelength of the X-ray radiation and θ is the Bragg angle. According to Eq. (1), the average crystallite size of the nanostructured YSZ powder is 34 nm.

2.2. Air plasma spraying

The coatings in the present study were made by a Metco A3000S atmospheric plasma spray system using a Sulzer-Metco F4-MB plasma gun (Sulzer Metco AG, Switzerland). The feedstock powders were fed with a Twin-system 10-C. Argon and hydrogen were the primary and secondary plasma gases, respectively. Also, argon gas was used as the carrier gas

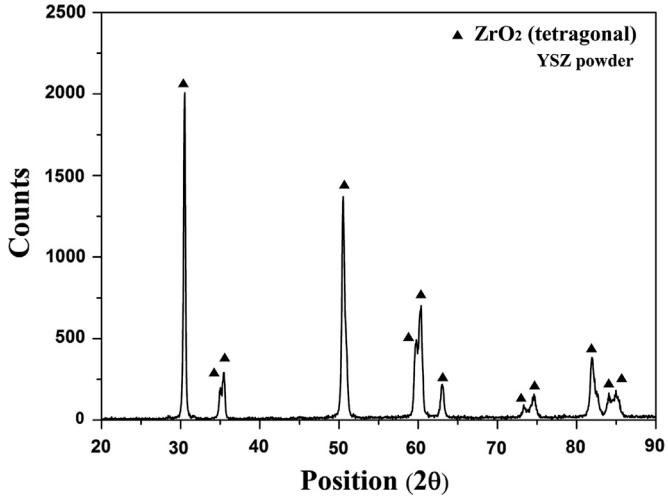

Fig. 2. XRD pattern of agglomerated nanostructured powder.

Table 1
Parameters of plasma spraying.

Parameter	NiCrAlY	Nanostructured YSZ
Current (A)	600	600
Voltage (V)	75	72
Primary gas, Ar (SLPM[a])	65	35
Secondary gas, H_2 (SLPM)	14	10
Carrier gas, Ar (SLPM)	2.3	3.5
Powder feed rate (g/min)	40	18
Spray distance (mm)	120	120

[a]Standard Liter Per Minute.

for transferring the powder particles for the powder supply to the plasma torch. The substrate surface was grit-blasted with 24 mesh alumina abrasive powder under a pressure of 5 bar and a distance of 10 cm, before applying coatings. The surface was then cleaned with acetone and preheated to provide ideal substrate bonding to the coating. The spraying parameters are listed in Table 1.

2.3. Laser glazing

Laser glazing was carried out on the surface of top coat by an Nd:YAG pulsed laser with the wavelength of 1064 nm, model PIM3475, mean power of 750 W and standard square shaped pulses. It can be pulsed at repetition rates ranging from 1 Hz up to 250 Hz. The system was also equipped with a powermeter (500 W-Lp Ophir) for power measurement and an *X–Y* table for accurate movement for the specimens. In order to cover the coating surface completely, the specimens were subjected to multiple scans with an overlap of 20% between consecutive tracks, always in the same direction. Laser glazing parameters are listed in Table 2.

2.4. Thermal insulation evaluation

In order to directly evaluate the thermal insulation capability of TBCs, the thermal insulation capability test was carried out by a

Table 2
Laser glazing parameters.

Parameter	Value
Average working power (W)	82
Pulsed frequency (Hz)	38
Scanning speed (mm/s)	15
Overlap (mm)	0.2
Distance (mm)	11

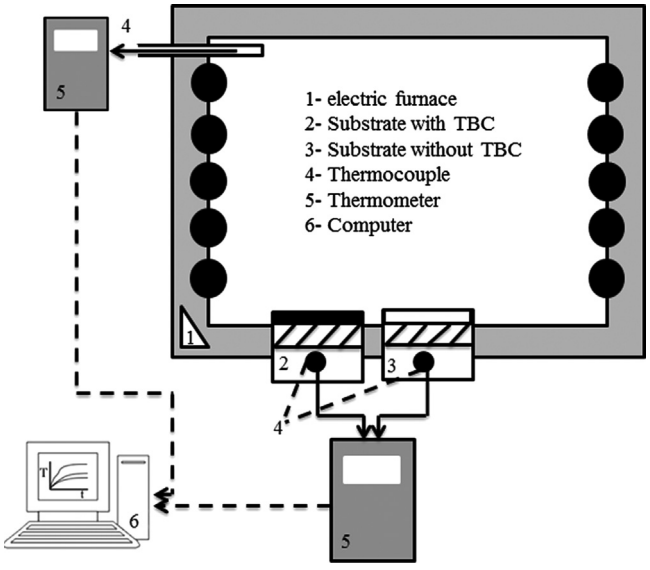

Fig. 3. Schematic illustration of the thermal insulation capability test.

self-developed device. This set-up was made with a temperature difference technique, as shown in Fig. 3. So, to eliminate the effect of temperature drop by substrate and cool the substrate backside by air, a similar substrate without TBC was used as the reference sample. Consequently, a TBC sample and a substrate sample were fixed in the electric furnace door. The surfaces of the TBC sample and the substrate sample were heated by the electric furnace and both sample backsides were in air. Three thermocouples were used as sensors. Thermocouple 1 was fixed inside the electrical furnace to monitor the furnace temperature (T_0). Thermocouple 2 and thermocouple 3 were fixed in both sample backsides to monitor the backside temperature of the coated sample (T_1) and the reference sample without TBC (T_2). The thermocouples were linked to a thermometer and then to a computer to record the heating temperatures. The average heating rate of the electric furnace was 15 °C/min. T_0, T_1 and T_2 records from the beginning of the test in 1-min intervals and *t–T* curves were plotted. When T_0 reached 1000 °C and T_1 and T_2 became stable, the thermal insulation capability by the temperature drop across TBC ($\Delta T = T_2 - T_1$) was calculated.

2.5. Specimens characterization

The microstructure of as-sprayed and laser-glazed coatings was determined by field emission scanning electron microscopy (FESEM; S-4160, Hitachi, Japan). The phase structure of the

starting powder, as-sprayed coating, and the laser-glazed coating was identified with a X-ray diffractometer (D8 ADVANCE, Bruker, Germany) using Cu Kα radiation (λ=0.15406 nm) produced at 40 KV and 40 mA. The surface roughness (Ra) of coatings was measured by a Mitutoyo Surftest profilometer (Mitutoyo SJ-201P, Japan) with a cut-off length of 800 μm and a measurement length of 8 mm. The roughness reported was the average of five values scanned from different areas on the coating surface.

3. Results and discussion

3.1. Microstructure of as-sprayed coating

The FESEM of polished cross-section of the as-sprayed coating is shown in Fig. 4. In this figure, different layers of TBC including NiCrAlY bond coat and nanostructured YSZ top coat can be observed. Thickness of top coat and bond coat is 300 ± 25 μm and 180 ± 25 μm, respectively. The surface morphology of as-sprayed nanostructured coating using FESEM is shown in Fig. 5(a). As can be seen, the microstructure of as-sprayed coatings is composed of two distinct structures. One is the continuous molten phase, which evolved from the fully molten part of the nanostructured YSZ agglomerated powders, and the other is non-molten and partial phase that retained the nanostructure of the starting powder. It can be seen that top surface of as-sprayed coating is very rough (Ra=9.20 μm) because partially molten particles involved in lower deformation impacted the surface as compared to fully molten particles [27–29]. Melted zone of top coat surface contained microcrack that was due to the thermal stress arising from rapid solidification of flatten particles [30,31]. Fig. 5(b) shows non-melted and partially molten zones of Fig. 5(a) at a higher magnification, similar to the starting powder.

Fig. 6 presents the fracture morphologies of as-sprayed nanostructured coating at different magnifications. These figures reveal a bimodal microstructure of as-sprayed coating consisting of microcolumnar grains formed from the resolidification of the molten part of the powder and the nanosized powder in the coating, which results from non-molten or partially molten part of the powders bonded by the molten part [32–34]. The pores and cracks in the splat structure are due to the residual stresses during the deposition process and presence of voids and pores can be attributed to the lack of complete overlap of adjacent splat and entrapment of the air during the plasma spraying

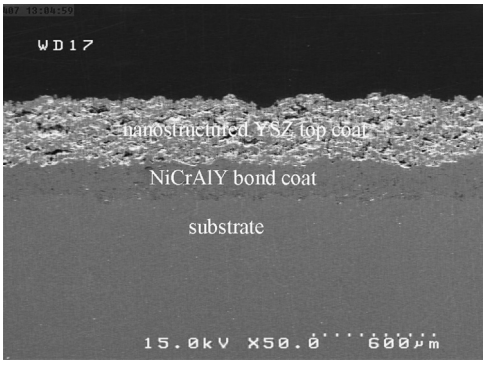

Fig. 4. FESEM micrograph of polished cross-section of the plasma-sprayed nanostructured YSZ thermal barrier coating.

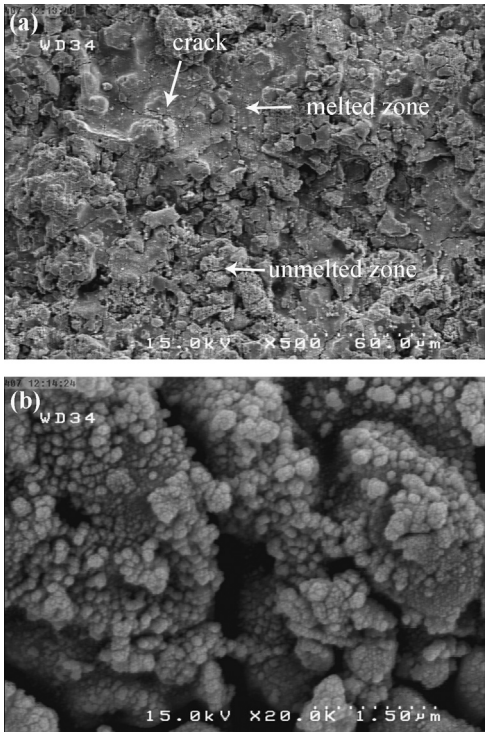

Fig. 5. FESEM micrographs of (a) top surface of the plasma-sprayed nanostructured coating and (b) partially melted zone at a higher magnification.

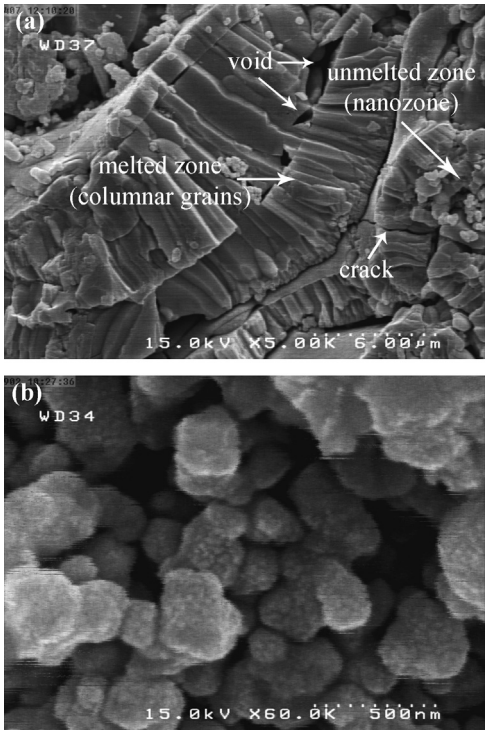

Fig. 6. FESEM micrographs of (a) fractured cross-section of the plasma-sprayed nanostructured coating and (b) non-molten nanoparticles within coating at a high magnification.

[27,35]. Fig. 6(b) shows that the initial nanostructure of powder is retained in the coating. This zone is called nanozone. It can be seen that the morphology of the nanozone is porous. The presence of crack, porosity and void has a significant effect on the TBC thermal conductivity [1,23].

3.2. Microstructure of laser glazed coating

Fig. 7 shows the surface morphology of laser-glazed coating. All the principal characteristics in the plasma-sprayed nanostructured TBCs such as cracks, voids, porosity, splats, protrusions, partially particles, and non-melted grains vanished after laser glazing. The surface roughness (Ra) of laser-glazed coating was 2.5 μm, which was significantly smaller than that of as-sprayed coating (9.20 μm). In laser glazing process, as the laser is moved, there is a temperature gradient between the laser beams and solidifying zone, generating a shear force on the liquid surface collated by surface tension forces. When the laser beam passed through the molten area, the temperature was uniform and gravity forces counteracted the external shear force, thus tending to restore the surface height of the molten zone. As the laser beam passed the region, this zone was solidified rapidly. These remelting and resolidification phenomena resulted in the reduction of surface roughness [23,25,36,37]. According to the previous [38] studies, reduction on the surface roughness leads to improvement of the erosion resistance. Fig. 7(b) shows a distinctively different microstructure of the glazed layer too. The coarse aquiaxial grain was nucleared at the surface and grew inward [39]. It can be seen from Fig. 7(a) that the bubbles were formed during laser glazing on the surface coating. As-sprayed ceramic top coat contains porosity and the ceramic melts, so these pores are coalesced, rising to the surface. A surface bubble is then formed when the ceramic resolidifies, before the pore has completely reached the surface [40,41].

Fig. 8 shows the fractured cross-section of laser-glazed coating at two magnifications. As shown in Figs. 8 and 9, the glazed layer consisted of a completely resolidified, dense microstructure and included segmented cracks. The net-shaped crack was created from the cooling process. This crack was propagated to the vertical direction from the surface. The crack depth of the sample was extended through the entire thickness of laser-glazed zone. Cracking, without any doubt, is due to shrinkage and thermal stresses developed during rapid solidification [42,43]. The formation of the segmented network of cracks in laser-glazed coating helps increase high thermal shock resistance and the thermal cycle life time [23,44,45]. High magnification micrograph of the glazed layer is shown in Fig. 8(b). In the melted region, the microstructure of the coating is homogeneous and the microcrack and pores are almost eliminated. Remelted surface by rapid melting and solidification resulted in a dense glazed layer. The microstructure of the glazed layers changed from lamellar to columnar due to the direction of the heat flow from cooling down to room temperature [46,47]. The sealing of surface pores prevents entrance of corrosive salts, thereby improving the hot corrosive resistance of the surface [17,48]. It is important to note that the columnar grain is more helpful in increasing operation stress and strain [46].

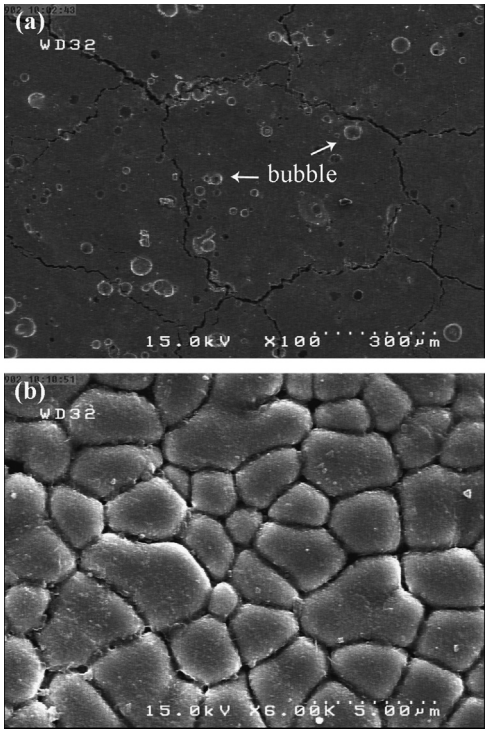

Fig. 7. FESEM micrographs of the laser-glazed coating; (a) upper surface view and (b) higher magnification showing the equiaxed grains.

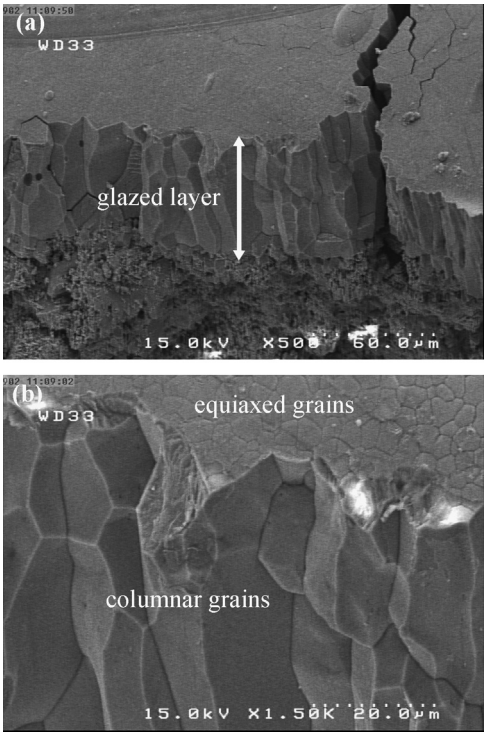

Fig. 8. FESEM micrographs of fracture cross-section of the laser-glazed coating at different magnifications.

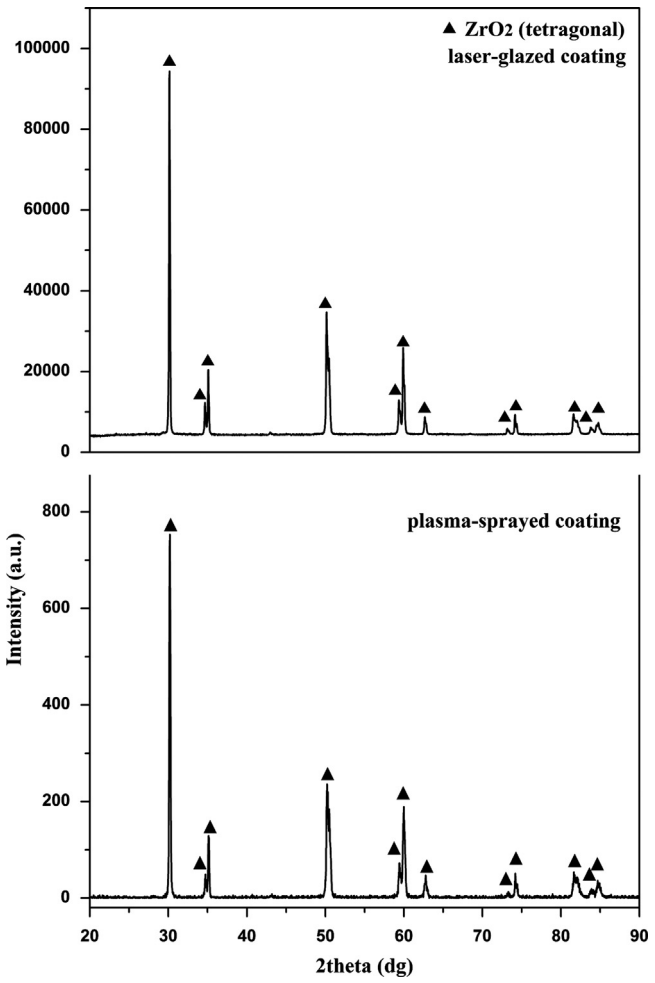

Fig. 9. XRD patterns of as-sprayed and laser-glazed nanostructured YSZ coating.

3.3. Phase analysis of coatings

Fig. 9 illustrates the XRD patterns of the as-sprayed and the as-glazed coating. It demonstrates that the phase composition of as-sprayed and as-glazed coatings was the non-transformable tetragonal phase (T′). This phenomenon resulted from the rapid solidification during the process of APS and laser glazing [36,49]. The cooling rate of the splats during the plasma spraying process and laser glazing was estimated to be 10^7 °C/s and 10^3–10^4 °C/s, respectively [45]. It can be seen from Fig. 9 that there are no new phases in the as-glazed coating as compared to the as-sprayed coating. The relative intensity of the individual diffraction peaks was greatly changed due to the glazing process. This is due to the change of microstructure. Particularly noteworthy was that the result of XRD analysis was consistent with the result of the surface and fracture microstructure of coating. The microstructure of the as-glazed coating was a combination of equiaxed grains on the top surface and columnar grains in the fracture surface. Increasing relative intensity peaks in the laser-glazed coating was due to the columnar grain orientation, which was caused by the laser glazing process [36,50].

3.4. Thermal insulation of coatings

Thermal barrier coatings are widely used in industrial gas-turbine engines. Therefore, studying the thermal insulation capability of the TBC is necessary to estimate their performance at temperature close to service conditions (1000–1100 °C). In this work, the thermal insulation capability of TBC was calculated by the temperature drop across TBC ($\Delta T=T_2-T_1$). The temperature drops across TBC were measured at 1000 °C and are shown in Fig. 10. It can be seen that the temperature drops of as-sprayed and glazed were 158 °C and 143 °C, respectively.

It is apparent that the thermal insulation of thermal barrier coatings strongly depends on the crystal structure and microstructure features, which result from the spraying process [27,51]. Microstructure of plasma-sprayed TBCs shows a two-dimensional microcrack; one inter-splat crack oriented parallel to the coating surface and intra-splat crack oriented perpendicular to the coating [52,53]. It is the parallel oriented cracks which are particularly effective in reducing the thermal conductivity (increasing thermal insulation capability) in the coating as the interfaces formed by such cracks are also perpendicular to the primary heat flux [54]. On the other hand, ceramic materials are thermal insulation inasmuch as they lack large numbers of free electrons. Thus, the phonons are primarily responsible for thermal conduction. Again, the phonons are not as effective as free electrons in the transport of heat energy as a result of the very efficient phonon scattering by lattice imperfection. The low thermal conductivity of YSZ is a result of the low intrinsic thermal conductivity of zirconia and the addition of yttria. Yttria addition requires the creation of O^{2-} vacancies to maintain the electrical neutrality of the ionic lattice. Both the yttrium solutes and the O^{2-} vacancies are effective at increasing phonon scattering in the lattice [55,56].

The observed difference in thermal insulation reported in this study can be explained by the microstructural change developed within the glazed-coating. The decrease in voids and microcracks in glazed-coating leads to the increase in apparent thermal conductivity and the decrease in thermal insulation. However, a fully dense, partly layered structure of top coat is helpful to improve corrosion, erosion and thermal shock resistance of TBCs.

4. Conclusion

The aim of this study was to evaluate the microstructure and thermal insulation capability of the laser-glazed plasma-sprayed thermal barrier coating; some important results can be summarized as follows:

- The nanostructured as-sprayed coating possessed a lamellar structure consisting of nanosized particles and microcolumnar grains. After laser glazing, all the principal characteristics present in the plasma-sprayed nanostructured TBCs vanished.
- The laser glazing process reduced the surface roughness, eliminated the porosity of surface and produced network cracks perpendicular to the surface.

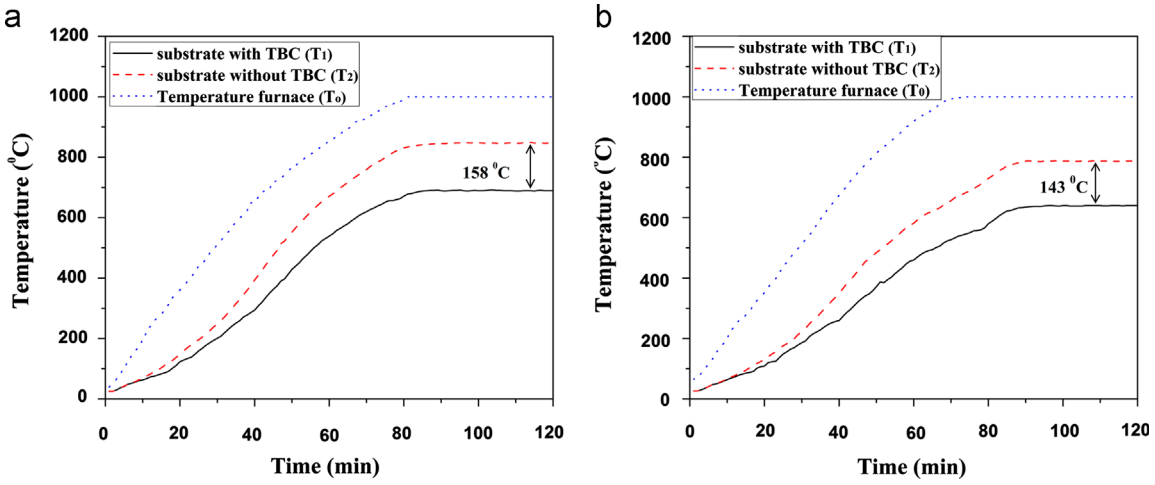

Fig. 10. Heating temperature curves of furnace and samples; (a) as-sprayed TBC and (b) laser-glazed TBC.

- The results of FESEM revealed that the microstructure of as-glazed coating could be altered from single columnar grains to a combination of columnar grains in the fracture and equiaxed grain on the surface.
- After laser glazing, the phase composition mainly consisted of non-transformable tetragonal phase (T′), the same as plasma sprayed phase composition.
- The experimental results of the thermal insulation capability test indicated that the as-glazed coatings possessed slightly lower thermal insulation as compared to the as-sprayed coatings due to the microstructural change in the glazed-layer of top coat.

Acknowledgments

This work was supported by the Malek-Ashtar University of Technology, Department of Materials Engineering. The authors would like to gratefully appreciate the contribution of Mrs. Raheleh Ahmadi-Pidani.

References

[1] H. Jamali, R. Mozafarinia, R. Shoja-Razavi, R. Ahmadi-Pidani, Comparison of thermal shock resistances of plasma-sprayed nanostructured and conventional yttria stabilized zirconia thermal barrier coatings, Ceramics International 38 (2012) 6705–6712.

[2] C.S. Ramachandran, V. Balasubramanian, P.V. Ananthapadmanabhan, Erosion of atmospheric plasma sprayed rare earth oxide coatings under air suspended corundum particles, Ceramics International 39 (2013) 649–672.

[3] R. Ahmadi-Pidani, R. Shoja-Razavi, R. Mozafarinia, H. Jamali, Evaluation of hot corrosion behavior of plasma sprayed ceria and yttria stabilized zirconia thermal barrier coatings in the presence of Na_2SO_4+V_2O_5 molten salt, Ceramics International 38 (2012) 6613–6620.

[4] S. Das, S. Datta, D. Basu, G.C. Das, Glass–ceramics as oxidation resistant bond coat in thermal barrier coating system, Ceramics International 35 (2009) 1403–1406.

[5] N. Wang, C. Zhou, S. Gong, H. Xu, Heat treatment of nanostructured thermal barrier coating, Ceramics International 33 (2007) 1075–1081.

[6] Y. Bai, L. Zhao, J.J. Tang, S.Q. Ma, C.H. Ding, J.F. Yang, L. Yu, Z.H. Han, Influence of original powders on the microstructure and properties of thermal barrier coatings deposited by supersonic atmospheric plasma spraying, part II: properties, Ceramics International 39 (2013) 4437–4448.

[7] C.R.C. Lima, N. Cinca, J.M. Guilemany, Study of the high temperature oxidation performance of thermal barrier coatings with HVOF sprayed bond coat and incorporating a PVD ceramic interlayer, Ceramics International 38 (2012) 6423–6429.

[8] L.I. Sun, H. Guo, H. Peng, S. Gong, H. Xu, Influence of partial substitution of Sc_2O_3 with Gd_2O_3 on the phase stability and thermal conductivity of Sc_2O_3-doped ZrO_2, Ceramics International 39 (2013) 3447–3451.

[9] H.J. Huang, M.C. Wang, The phase formation and stability of tetragonal ZrO_2 prepared in a silica bath, Ceramics International 39 (2013) 1729–1739.

[10] S. Das, S. Datta, D. Basu, G.C. Das, Thermal cyclic behavior of glass–ceramic bonded thermal barrier coating on nimonic alloy substrate, Ceramics International 35 (2009) 2123–2129.

[11] M. Abbas, H. Guo, M.R. Shahid, Comparative study on effect of oxide thickness on stress distribution of traditional and nanostructured zirconia coating systems, Ceramics International 39 (2013) 475–481.

[12] Y. Li, Y. Xie, L. Huang, X. Liu, X. Zheng, Effect of physical vapor deposited Al_2O_3 film on TGO growth in YSZ/CoNiCrAlY coatings, Ceramics International 38 (2012) 5113–5121.

[13] C. Chen, H. Guo, S. Gong, X. Zhao, P. Xiao, Sintering of electron beam physical vapor deposited thermal barrier coatings under flame shock, Ceramics International 39 (2013) 5093–5102.

[14] S. Guo, Y. Kagawa, Isothermal and cycle properties of EB-PVD yttria-partially-stabilized zirconia thermal barrier coatings at 1150 and 1300 °C, Ceramics International 33 (2007) 373–378.

[15] B. Liang, Chuanxian Ding, Thermal shock resistances of nanostructured and conventional zirconia coatings deposited by atmospheric plasma spraying, Surface and Coatings Technology 197 (2005) 185–192.

[16] C. Zhou, N. Wang, H. Xu, Comparison of thermal cycling behavior of plasma-sprayed nanostructured and traditional thermal barrier coatings, Materials Science and Engineering A 452–453 (2007) 569–574.

[17] P.C. Tsai, J.H. Lee, C.S. Hsu, Hot corrosion behavior of laser-glazed plasma-sprayed yttria-stabilized zirconia thermal barrier coatings in the presence of V_2O_5, Surface and Coatings Technology 201 (2007) 5143–5147.

[18] K. Kokini, Y.R. Takeuchi, B.D. Choules, Thermal crack initation mechanisms on the surface of functionally graded ceramic thermal barrier coatings, Ceramics International 22 (1996) 397–401.

[19] S. Ahmaniemi, J. Tuominen, M. Vippola, P. Vuoristo, T. Mäntylä, F. Cernuschi, C. Gualco, A. Bonadei, R. Di Maggio, Characterization of modified thick thermal barrier coatings, Journal of Thermal Spray Technology 13 (2004) 361–370.

[20] R. Ahmadi-Pidani, R. Shoja-Razavi, R. Mozafarinia, H. Jamali, Laser surface modification of plasma sprayed CYSZ thermal barrier coatings, Ceramics International 39 (2013) 2473–2480.
[21] J.H. Ouyang, S. Nowotny, A. Richter, E. Beyer, Laser cladding of yttria partially stabilized ZrO_2 (YPSZ) ceramic coatings on aluminum alloys, Ceramics International 27 (2001) 15–24.
[22] G. Zhang, Y. Liang, Yi Wu, Z. Feng, B. Zhang, Laser remelting of plasma sprayed thermal barrier coatings, Journal of Materials Sciences and Technology 17 (2001) 105–110.
[23] R. Ahmadi-Pidani, R. Shoja-Razavi, R. Mozafarinia, H. Jamali, Improving the thermal shock resistance of plasma sprayed CYSZ thermal barrier coatings by laser surface modification, Optics and Lasers in Engineering 50 (2012) 780–786.
[24] S. Ahmaniemi, P. Vuoristo, T. Mäntylä, Mechanical and elastic properties of modified thick thermal barrier coatings, Materials Science and Engineering A 366 (2004) 175–182.
[25] C. Batista, A. Portinha, R.M. Ribeiro, V. Teixeira, M.F. Costa, C. R. Oliveira, Morphological and microstructural characterization of laser-glazed plasma-sprayed thermal barrier coatings, Surface and Coatings Technology 200 (2006) 2929–2937.
[26] K.K. Szkaradek, Laser melted ZrO_2–Y_2O_3 thermal barrier obtained by plasma spraying method, Journal of Alloys and Compounds 505 (2010) 516–523.
[27] H. Jamali, R. Mozafarinia, R. Shoja Razavi, R. Ahmadi-Pidani, M.R. Loghman-Estarki, Fabrication and evaluation of plasma-sprayed nanostructured and conventional YSZ thermal barrier coatings, Current Nanoscience 8 (2012) 402–409.
[28] G.D. Girolamo, F. Marra, C. Blasi, E. Serra, T. Valente, Microstructure, mechanical properties and thermal shock resistance of plasma sprayed nanostructured zirconia coatings, Ceramics International 37 (2011) 2711–2717.
[29] D. Seo, K. Ogawa, T. Shoji, S. Murata, Effect of particle size distribution on isothermal oxidation characteristics of plasma sprayed CoNi- and CoCrAlY coatings, Journal of Thermal Spray Technology 16 (2007) 954–966.
[30] S. Bose, High Temperature Coatings, Elsevier Science & Technology Books, Connecticut, USA, 2007.
[31] R.C. Reed, The Superalloys, Fundamentals and Applications, Cambridge University Press, Cambridge, 2006.
[32] J. Sun, L. Zhang, D. Zhao, Microstructure and thermal cycling behavior of nanostructured yttria partially stabilized zirconia (YSZ) thermal barrier coatings, Journal of Rare Earths 28 (2010) 198–201.
[33] X. Jiang, C. Liu., F. Lin, Overview on the development of nanostructured thermal barrier coatings, Journal of Materials Sciences and Technology 23 (2007) 449–457.
[34] R.S. Lima, B.R. Marple, Thermal spray coatings engineered from nanostructured ceramic agglomerated powders for structural, thermal barrier and biomedical applications: a review, Journal of Thermal Spray Technology 16 (2007) 40–63.
[35] H. Chen, Y. Zeng, C. Ding, Microstructural characterization of plasma-sprayed nanostructured zirconia powders and coatings, Journal of the European Ceramic Society 23 (2003) 491–497.
[36] C. Batista, A. Portinha, R.M. Ribeiro, V. Teixeira, M.F. Costa, C.R. Oliveira, Surface laser-glazing of plasma-sprayed thermal barrier coatings, Applied Surface Science 247 (2005) 313–319.
[37] G. Strano., L. Hao, R.M. Everson, K.E. Evans, Surface roughness analysis, modelling and prediction in selective laser melting, Journal of Materials Processing Technology 213 (2013) 589–597.
[38] P.C. Tsai, J.H. Lee, C.L. Chang, Improving the erosion resistance of plasma-sprayed zirconia thermal barrier coatings by laser glazing, Surface and Coatings Technology 202 (2007) 719–724.
[39] G. Antou, G. Montavon, F. Hlawka, A. Cornet, C. Coddet, F. Machi, Processing of yttria partially stabilized zirconia thermal barrier coatings implementing a high-power laser diode, Journal of Thermal Spray Technology 13 (2004) 381–389.
[40] F.J. Ester, A. Larrea, R.I. Merino, Processing and microstructural study of surface laser remelted Al_2O_3–YSZ–YAG eutectic plates, Journal of the European Ceramic Society 31 (2011) 1257–1268.
[41] B.S. Yilbas, A.F.M. Arif, M.A. Gondal, HVOF coating and laser treatment: three-point bending tests, Journal of Materials Processing Technology 164–165 (2005) 954–957.
[42] C. Zhu, P. Li, A. Javed, G.Y. Liang, P. Xiao, An investigation on the microstructure and oxidation behavior of laser remelted air plasma sprayed thermal barrier coatings, Surface and Coatings Technology 206 (2012) 3739–3746.
[43] H.V. Pokhmurs'ka, Crack formation in gas-thermal coatings depending on the conditions of their laser remelting, Materials Science 39 (2003) 64–68.
[44] M.J. Kadhim, Laser sealing and thermal shock resistance of 6.5 wt% yttria partially stabilized zirconia plasma sprayed layers, Engineering and Technology Journal 27 (2009) 1038–1045.
[45] J.H. Lee, P.C. Tsai, C.L. Chang, Microstructure and thermal cyclic performance of laser-glazed plasma-sprayed ceria–yttria-stabilized zirconia thermal barrier coatings, Surface and Coatings Technology 202 (2008) 5607–5612.
[46] H. Chen, Y. Hao, H. Wang, W. Tang, Analysis of the microstructure and thermal shock resistance of laser glazed nanostructured zirconia TBCs, Journal of Thermal Spray Technology 19 (2010) 558–565.
[47] G. Antou, G. Montavon, F. Hlawka, A. Cornet, C. Coddet, F. Machi, Modification of ceramic thermal spray deposit microstructures implementing in situ laser remelting, Surface and Coatings Technology 172 (2003) 279–290.
[48] P.C. Tsai, C.S. Hsu, High temperature corrosion resistance and microstructural evaluation of laser-glazed plasma-sprayed zirconia MCrAlY thermal barrier coatings, Surface and Coatings Technology 183 (2004) 29–34.
[49] K.Mohammed Jasim, Characterization of laser sealed coatings of yttria partially stabilized zirconia, Optics and Lasers in Engineering 49 (2011) 785–792.
[50] S. Ahmaniemi, J. Tuominen, P. Vuoristo, T. Mantyla, Sealing procedures for thick thermal barrier coatings, Journal of Thermal Spray Technology 11 (2002) 320–332.
[51] L. Wang, Y. Wang, X.G. Sun, J.Q. He, Z.Y. Pan, Y. Zhou, P.L. Wu, Influence of pores on the thermal insulation behavior of thermal barrier coatings prepared by atmospheric plasma spray, Materials and Design 32 (2011) 36–47.
[52] K.W. Schlichting, N.P. Padture, P.G. Klemens, Thermal conductivity of dense and porous yttria-stabilized zirconia, Journal of Materials Science 36 (2001) 3003–3010.
[53] R. Ghasemi, R. Shoja-Razavi, R. Mozafarinia, H. Jamali, Comparison of microstructure and mechanical properties of plasma-sprayed nanostructured and conventional yttria stabilized zirconia thermal barrier coatings, Ceramics International (2013), 10.1016/j.ceramint.2013.04.068.
[54] N.P. Padture, M. Gell, L. Eric, H. Jordan, Thermal barrier coatings for gas turbine engine applications, Materials Science 296 (2002) 280–285.
[55] P.G. Klemens, M. Gell, Thermal conductivity of thermal barrier coatings, Materials Science and Engineering A 245 (1998) 143–149.
[56] J.R. Nicholls, K.J. Lawson, A. Johnstone, D.S. Rickerby, Methods to reduce the thermal conductivity of EB-PVD TBCs, Surface and Coatings Technology 151–152 (2002) 383–391.